Journal of Civil Structural Health Monitoring
https://doi.org/10.1007/s13349-024-00864-z

ORIGINAL PAPER

Synchronous LoRa sensor nodes for modal identification in footbridge vibration monitoring

Huiyue Qiao[1] · Hong Guan[1] · Andrei Jabbour[1] · Yong Zhu[1]

Received: 31 May 2024 / Accepted: 25 September 2024

Abstract
This article aims at presenting a preliminary investigation of using long-range and low-cost LoRa (Long Range) technology and two synchronous LoRa sensor nodes for cost-effective footbridge structural health monitoring (SHM). Two sensor nodes with LoRa modules and accelerometers were employed for vibration monitoring and a new attempt was made to use synchronous LoRa nodes for modal identification. In this article, a modal identification method based on a lightweight synchronization concept was proposed. This method is able to identify the fundamental mode of vibrating beam structures. Meanwhile, maximum accelerations can also be tracked periodically from the simultaneously recorded acceleration data by the synchronous LoRa nodes. Specifically, synchronization was achieved through the wireless peer-to-peer (P2P) communication between the two LoRa nodes, with the aim of initializing simultaneous acceleration recordings. The fundamental frequency and the phase information derived from the on-board calculation of the synchronized nodes can then be used to effectively identify the vertical bending mode and torsion mode. A series of laboratory tests were also conducted on a beam structure for the purpose of validation. The test results showed that the fundamental mode of the vibrating beam can be obtained rapidly and accurately using the synchronized LoRa nodes, with an average synchronization accuracy of 4.45 ms. The maximum acceleration data recorded by the LoRa nodes also showed high accuracy when compared with the raw acceleration data collected from a commercial Bluetooth accelerometer node. The fundamental frequencies obtained from both types of nodes also compare reasonably. The proposed modal identification method using two synchronous LoRa sensor nodes provides a basis for the development of a low-cost footbridge SHM system with the integration of IoT techniques. An attempt has been made to perform a preliminary field test on a cable-stayed footbridge, where the fundamental frequency and the mode shape type of the footbridge were successfully identified and its serviceability condition was also found to satisfy the code requirements.

Keywords LoRa · Network synchronization · Footbridge · SHM · Vibration monitoring · Modal identification

1 Introduction

1.1 Current research advances and challenges for vibration-based footbridge SHM

Structural health monitoring (SHM) works as a promising strategy to track the overall performances of structures under their operating conditions, which helps to provide timely warning for structural damages and deteriorations. Vibration-based monitoring is the primary monitoring technique in bridge SHM, which focuses on measuring and analyzing the vibration activities of structures under service loads. In this way, key modal parameters can be extracted from the measured acceleration data, including the natural frequencies, mode shapes and damping ratios. These parameters are all inherent modal characteristics of a bridge and are dependent only on the construction material properties and damping capacity of the structure, regardless of any external excitations. By investigating the changes of these modal parameters during the service life of a bridge, structural health condition and operational performances of the bridge can be monitored, allowing for the timely acquisition of deterioration and/or early-stage damage warning information.

Vibration-based bridge SHM systems have been widely implemented on long-span vehicle bridges [1], where the

✉ Hong Guan
h.guan@griffith.edu.au

[1] School of Engineering and Built Environment, Griffith University, Gold Coast Campus, Southport, QLD, Australia

Published online: 05 October 2024

majority have followed a traditional method by deploying multiple wire-connected accelerometers on the bridges. Subsequently, a large amount of monitoring data can be collected from several parts of a bridge to attain a comprehensive acceleration measurement, and all the data can be transmitted to a base station for an inclusive post-analysis. Although bridge failure only happens in very low probability, the consequence of failure can be rather severe, causing economic losses and human casualties [2]. As a primary cause of failures, structural deterioration has caused collapse of the Nanfang'ao Bridge in Taiwan, China [3], the Morandi Bridge in Genoa, Italy [4], and the Fern Hollow Bridge in Pittsburgh, USA [5] in recent years. SHM systems play an important role in tracking and evaluating the structural conditions of bridges in a timely manner, thereby preventing catastrophic failure. Hence, implementing SHM systems on bridges can be beneficial for bridge management from the safety and long-term performance perspectives. This takes into account the uncertainty in the maintenance planning of bridges and the serious economic consequences due to the delayed detection of structural health problems in bridges [2]. However, for footbridges with relatively smaller scales and loading requirements, deploying traditional wired SHM systems with base stations can be less economical when considering the initial expenses on labor and devices. Nevertheless, when it comes to footbridges that exhibit poor serviceability or questionable structural conditions, timely modal identification and acceleration monitoring are crucial, as this takes into consideration the safety concerns for both pedestrians and structures. As such, more cost-effective solutions should be implemented for footbridge modal identification and acceleration monitoring, which would be beneficial to attain low-cost sensor network deployment, maintenance, and data transmission, as well as to achieve high automation of the monitoring systems.

To be specific, footbridges with apparent slenderness may exhibit excessive vibrations under human-induced vibrations [6], as are the ones with design deficiencies. This problem can be raised especially when the fundamental frequencies of footbridges approach the range of the walking frequencies of pedestrians, where resonant vibration phenomena present. In the meantime, aged bridges may exhibit safety issues due to structural deterioration as well [7]. Therefore, conforming to the existing footbridge serviceability evaluation requirements, SHM systems for footbridges should be able to capture and track the fundamental frequency of footbridges during their operation lifetime, as well as to record the acceleration-related parameters derived from the processed raw acceleration data [8].

With regard to the research advances for footbridge SHM systems in the nearest decade, many wired data acquisition systems have been employed for the continuous monitoring of the dynamic behaviors of footbridges [9–14]. Among these studies, long-term changes in modal parameters like fundamental frequency and damping ratio have been investigated with or without considering the effects of temperature and wind. Moreover, continuous acceleration monitoring also plays an important role in the design of these SHM systems. However, it can be very costly to promote full implementation of wired SHM systems for footbridges, considering the time and economic costs of wire deployment, base station construction, and any possible manual data collection and maintenance activities. To address these issues, modal identification using wireless sensor nodes has been adopted in footbridge applications, where successive vibration records can be forwarded wirelessly from sensor nodes to a base station [15] or to devices like gateways or laptops that relay central network connections [16, 17]. Thus, wired system deployment is avoided, and even the establishment of a base station is not compulsory. However, a primary concern is that since modal identification requires adequate amount of acceleration data all over a bridge, wirelessly transmitting enormous amounts of raw data from senor nodes to a centralized data processing destination would require significant power from the wireless sensor node layer. This can challenge the operation time of the wireless sensor nodes. As a result, some researches on footbridge wireless SHM have investigated a solution by adopting local data processing with embedded algorithms on the wireless sensor nodes. In doing so, the amount of data to be transmitted wirelessly can be significantly reduced [18, 19]. However, among the current practices of wireless footbridge SHM systems utilizing centralized or local data processing for modal identification, their transmission protocols employed are either short-range ones (e.g., Wi-Fi or Bluetooth) or costly ones (3G or 4G). These would either limit the transmission range or add extra service charges for remote monitoring. Consequently, for a practical implementation of modal identification in wireless footbridge SHM, two key factors should be considered: (1) local data processing on the sensor node to reduce the power consumption in wireless data transmission; (2) low-cost and long-range wireless transmission protocols to minimize the remote data transmission service charges.

1.2 Applications of *LoRa* technology in bridge SHM

To achieve the best cost-effectiveness in the data transmission of footbridge SHM, long-range and low-cost protocols like Narrowband Internet of Things (NB-IoT) and LoRa Wide Area Networking (LoRaWAN) can be adopted. Compared to NB-IoT, LoRaWAN has a smaller data rate but is characterized by even lower energy consumption in data transmission and larger scalability for deploying wireless sensor networks (WSNs). In addition, unlike NB-IoT, LoRaWAN operates in unlicensed frequency bands,

allowing for more flexible and easier network deployment without requiring specific licensing arrangements [20]. Typically, LoRaWAN is a medium access control (MAC) layer protocol designed by the LoRa Alliance built on top of the LoRa physical layer [21], instructing and coordinating the activities of LoRa devices. In the LoRa physical layer, LoRa technology applies chirp spread spectrum, allowing peer-to-peer (P2P) communication between LoRa end devices in a LoRa WSN. Further, LoRaWAN can create a link for the LoRa gateway and LoRa end devices, as the data from the end devices can be directed to centralized network by LoRa gateways [22]. Therefore, LoRa technology helps achieving super-long-range remote monitoring systems, enabling notable long-distance wireless data transmission for the P2P communication among LoRa devices as well as for the LoRaWAN communication between gateways and end devices. In particular, the data transmission range can exceed several kilometers, relying on the device capabilities, gateway range, network topology, interferences and so on. Given all these advantages, it would be possible to use the LoRa technique to realize long-range wireless footbridge monitoring while minimizing the cost on wireless data transmission.

Notably, LoRa technology is suitable for remote monitoring where a small amount of data is transmitted. This technology has been used to perform long-distance transmission for structural performance and climate information in bridge SHM. For example, Sidorov et al. [23] proposed a remote monitoring system that can be implemented on bridges to track the looseness of bolted joints, based on the pre-tensioned forces and temperatures collected by the strain sensor nodes. By taking advantage of LoRa technology, the minimum transmission distance of the sensor nodes can reach 3.8 km, with an estimated battery life of more than five years. Another distributed bridge SHM system using LoRa technology was investigated by Hou and Bao [20], where multiple pieces of information like bridge crack, displacement, temperature, humidity, tilt angles, timestamps, and more can be collected from the end sensor nodes and sent to the monitoring center. Other cases of using LoRa technology in bridge SHM to achieve long-range and low-power information acquisition have also been found in the research work of Truong et al. [24]. Despite these research efforts, little work has been conducted on using LoRa technology in vibration-based bridge SHM, likely due to two possible reasons. First, a basic modal identification requires abundant raw acceleration data; however, it can be challenging to transmit large amounts of raw data by LoRa technique, given its relatively low data rate and limited bandwidth. Second, synchronized data acquisition is a precondition for modal analysis; therefore, time synchronization also needs to be addressed for synchronous data collection from LoRa WSN.

The drawback of the narrow bandwidth of LoRa technology in raw acceleration data transmission can be addressed by employing on-board data computation. This approach has been practiced by transferring time-domain data into frequency results [25, 26]. This also conforms to the opinion that employing local data processing on sensor nodes in footbridge SHM can help reduce power consumption during wireless data transmission. Additionally, techniques like data compression and duty cycle increase have also been used to obtain adequate daily acceleration data for precise modal analysis on the cloud [27]. In this study, to optimize the energy cost in transmission, the on-board signal processing was adopted based on our preliminary research on using LoRa sensor nodes in beam vibration monitoring [26].

1.3 Existing *LoRa* synchronization techniques in WSNs

To address the other concern of using synchronized LoRa sensor nodes for modal identification, synchronous measurement needs to be attained among wireless LoRa sensor nodes. Synchronous measurement is a prerequisite for modal parameter identification in vibration-based SHM systems when multiple sensor nodes are used, and desynchronization may lead to inaccuracy when constructing mode shapes [28]. However, in LoRa WSNs connected to the centralized network using the LoRaWAN protocol, it can be difficult to achieve time synchronization since LoRaWAN does not have any time synchronization mechanism [29]. Thus, GPS modules have been employed in LoRa WSNs to receive coordinated universal time (UTC) stamps from satellites as standard time references, to regulate the time information for end devices [30, 31]. GPS synchronization can provide direct accuracy in timestamps, but additional hardware is also required, which would subsequently lead to more cost and power consumption on sensor nodes. In addition, GPS signals may exhibit inconsistency in wireless transmission in changeable outdoor environments.

Another approach to attaining synchronous LoRa WSNs is based on the LoRa MAC layer, where gateways tend to be used to schedule downlinks to the end nodes for real-time clock (RTC) offset correction in reference to the timestamp of the gateway [32]. Similarly, uplink and downlink transmissions between the gateway and the end nodes have also been used to exchange important time-related information in between [33]. As to the MAC layer time synchronization schemes, end nodes can receive unified order or time information from gateways directly without additional GPS chips. However, in consideration of their application in modal identification, continuous synchronization may be required to correct accumulating action latency among the end nodes over time. In this way, a

certain amount of energy is nonetheless required for frequent message transmissions between the gateway and the end devices. Such an energy consumption is also hardly aligned with the design basics of LoRa WSNs, where power cost efficiency is of paramount importance. Meanwhile, expected smooth packet transmission between the end nodes and the gateway may also be affected by multiple factors like network congestion, transmission distances, obstacles, and more, which would affect the stability of any subsequent synchronous measurement activities of the end node.

As a consequence, lightweight time synchronization methods are required when applying LoRa technology in bridge modal identification. Some existing time synchronization methods have been used for peer-to-peer (P2P) communication among LoRa end devices. For example, Tessaro et al. [34] used a master node to periodically broadcast timestamps to the rest of the end nodes in a LoRa WSN, and in this way, the synchronization error of the end nodes can be monitored under a threshold checking up to 4.5 ms every 10 s. Their methods may be suitable for WSN with multiple end nodes, but the synchronization process depends on the self-synchronization algorithm of the end nodes and may lack time efficiency at the application level. Another time synchronization strategy focused on two end devices was proposed by Singh et al. [29], where a reference timestamp of the master node is sent to the slave node, and the synchronization error caused by hardware discrepancy-related transmission time and board computation time can be compensated by a re-synchronization process with a resolution of up to 10 ms. This end-device-based time synchronization method is more convenient than those developed on the MAC layer, but it also requires network connection to the end nodes for reference RTC requisition, and attention is needed to format a suitable payload with an appropriate size for RTC. Gao et al. [35] also adopted the communication between sensor nodes and gateway nodes to synchronize sensor node clusters in machine vibration monitoring, where a gateway node takes charge of receiving adjacent timestamps from each sensor node in a cluster to determine the synchronization error for time compensation. Their method can attain a high synchronization resolution of up to 2 μs and is suitable for periodical synchronization for the elimination of time drift among sensor nodes as well as the clock time drift occurring in each sensor node. However, this method requires multiple timestamps and calculations for time compensation, which rely heavily on orderly LoRa packet transmission and therefore add complexity to the sensor node software operation. For the lightweight synchronization methods introduced above, the most relevant work is from Gao et al. [35], where a LoRa synchronization strategy was proposed for machine vibration monitoring with natural frequencies being obtained. Such a research effort has yet to be extended for bridge vibration monitoring. The challenges of mode shape identification and the application of LoRa synchronization methods for outdoor environment need to be addressed.

1.4 Aims of this study

With an emphasis on proposing a cost-effective and efficient modal identification method for footbridge SHM, this research, for the first time, adopted a lightweight synchronization strategy using P2P communication between two LoRa sensor nodes. An innovative attempt was made to use synchronous LoRa nodes for dynamic behavior monitoring of a beam structure in the laboratory and a cable-stayed footbridge in the field. The LoRa nodes are programmed specifically targeting the vertical vibrations in footbridges, where continuous modal identification and maximum acceleration amplitude tracking can be performed using locally processed results from LoRa nodes. In detail, two critical modal parameters can be obtained by the proposed modal identification method, including the fundamental frequency and the corresponding mode shape type. These modal parameters can be derived from the fast Fourier transform (FFT) algorithm and the phase correlation between the signals recorded by the two synchronized LoRa nodes. In this way, a fundamental mode can be confirmed by the peak frequencies and the phase difference from the two signals recorded by two LoRa nodes. A series of laboratory tests was performed to implement this modal identification method on a beam structure, and various fundamental modes of the vibrating beam with different support and excitation conditions were detected, including a pure vertical bending mode, a pure torsion mode and a mixed mode. The validity of LoRa nodes was also compared with a Bluetooth sensor when the beam was oscillating in the mixed mode. Upon connecting to the network infrastructure, the synchronous LoRa nodes were integrated with IoT techniques to perform a field test on the cable-stayed footbridge, from which the fundamental mode under its operating condition was identified. The IoT system enabled to upload the locally processed data results as LoRa packets to a cloud platform via the LoRaWAN network, serving as a pilot study for long-distance, low-power remote vibration monitoring for footbridges.

2 Design methodology

2.1 Modal identification method based on synchronized *LoRa* sensor nodes

A modal identification method, requiring two synchronous LoRa sensor nodes, was proposed for a low-cost IoT-based footbridge vibration monitoring system. This modal identification method aims at determining the fundamental

frequency as well as the corresponding mode shape type at regulated intervals for footbridges. Either of the LoRa node contains an Arduino MKRWAN1310, an ADXL335 accelerometer, and a dipole pentaband antenna. MKRWAN1310 can offer local data processing for temporarily stored acceleration samples within the capacity of its flash memory up to 256 KB. The embedded CMWX1ZZABZ radio module of MKRWAN1310 also enables P2P communication between nodes with the help of local LoRa signals, which is beneficial for the establishment of a lightweight synchronization protocol for synchronous data sampling prior to modal identification. The action flow of the two LoRa nodes is shown in Fig. 1. After calibration, two LoRa nodes start synchronization process and on-board data processing, which contains synchronous acceleration sampling and FFT calculation. Critical modal parameters like fundamental frequency and phase can thus be collected. As such, the proposed modal identification method can be used as an alternative to the Operational Modal Analysis (OMA), a popular vibration-based modal identification technique for bridge SHM.

Together with the consideration of footbridge serviceability evaluation, maximum acceleration is also anticipated as one of the outputs of the LoRa nodes, together with fundamental frequency and phase information during a specific sampling time. These results can be obtained as a result group from both sensor node 1 (S1) and sensor node 2 (S2) per software loop following the synchronized sampling and on-board calculation procedures, as indicated in Fig. 1. To perform modal identification, the fundamental frequencies and the phase difference between their phase results can be used to determine the fundamental vibration mode. In this study, two sensor nodes were adopted to test the applicability of the proposed synchronization and modal identification method, with more nodes being integrated in future studies. In detail, when positioning the two sensor nodes symmetrically on the opposite edge of the bridge deck, a bending mode is always aligned with a phase difference close to 0 between the collected signals from two nodes, whereas a torsion mode always corresponds to a phase difference near π. Hence, the phase difference information is used for rapid confirmation of the fundamental mode. It can also be used as a reflection indicator for the accuracy of the synchronization process. For the synchronization strategy employed in this research, the capacity of wireless communication between LoRa nodes was exploited, without a need of recording or processing the time drifts between nodes. Detailed explanation will be given for this synchronization method in Sect. 2.2.

2.2 Synchronization of *LoRa* nodes

As shown in Fig. 2, detailed synchronization procedures are presented in a single loop plot of the action flow of LoRa nodes, in accordance with every loop indicated in Fig. 1. After the LoRa nodes complete their calibration steps, S1 sends out a synchronization request packet to S2 in the very first step. At the same time, S2 is in a listen state for the request packet coming from S1. This request packet contains a string message "SYNC_REQUEST", and S2 would parse and read this packet before operating its next step. Only when S2 confirms that the content of the packet from S1 indicates a synchronization request, then it will generalize a confirmation packet to send back to S1. After that, S2 would recognize itself as synchronized with S1, by printing "Synched" and start recording accelerations. Compared with S2, one more step is required in S1 before commencing the acceleration sampling, as S1 needs to wait for the confirmation packet from S2, and the time limit of this waiting time was set as 10 ms to avoid synchronization errors caused by packet loss. If any packet is received within the 10 ms limit, S1 would parse it and check the content as "SYNC_RESPONSE" before printing "Synched". Consequently, there can be a possibility that S2 starts data sampling earlier than S1, where the time shift is approximately one-way transmission time for the confirmation packet from S2 to S1, depending on the signal conditions of LoRa and the processing time of sensor nodes. Any packet loss in between the synchronization procedures would trigger the judgment algorithm in the program to indicate synchronization failure and the synchronization process would subsequently restart all over again.

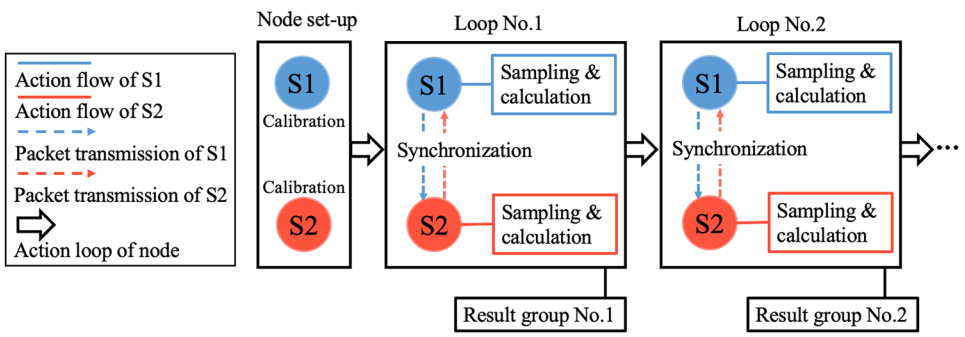

Fig. 1 Action flow chart of synchronous LoRa sensor nodes

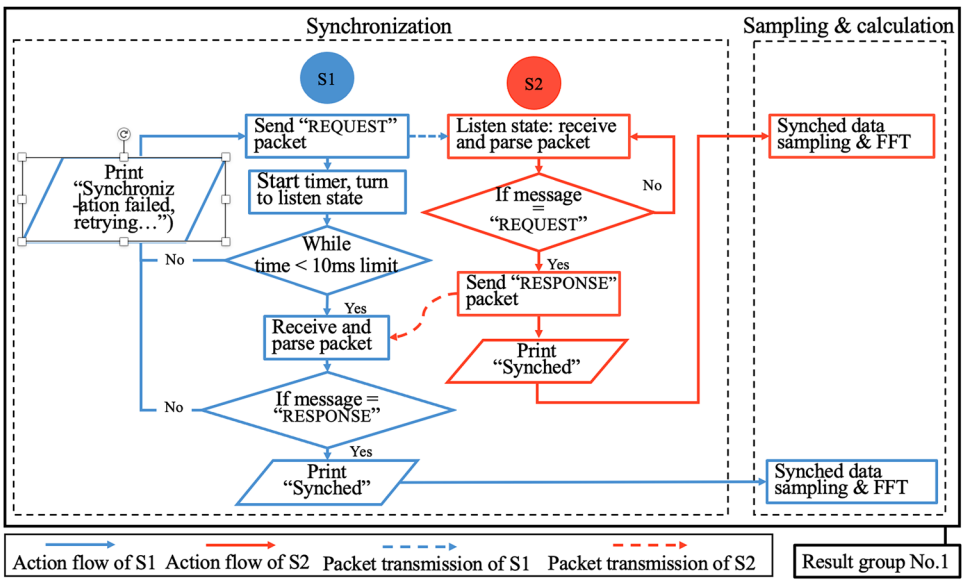

Fig. 2 Synchronization of LoRa nodes in one loop

In relation to the modal identification method introduced in Sect. 2.1, the inherent synchronization error may lead to slightly uncertain phase difference results compared with the ideal ones. For example, if the shape correlation of the recorded acceleration signals conforms to that indicated in Fig. 3, the phase difference can be drifted away from 0 and π in the vertical bending mode identification and torsion mode identification, respectively. The time error in imperfect synchronous data sampling may also be identified by other reasons, uncovered through trails. Possible reasons may include missing LoRa packets, and different processing time of microcontrollers of S1 and S2 for the "print" function. Therefore, it would not always be S2 to start an earlier data sampling.

If the time error is caused only by the additional packet transmission time in the confirmation signal reception part of S1, it can be neglected in this study, as the distance between the two LoRa nodes is sufficiently small (85 cm) in the experimental test. Even for any future deployment of LoRa nodes on footbridges, the distance up to one kilometer between the two sensor nodes will not affect the synchronization accuracy, as the speed of LoRa P2P communication is influenced by the quality of LoRa signals and the size of the confirmation packet. Uncertainty in the LoRa signal quality might induce packet loss as the communication distance increases, which can thus affect the synchronization efficiency. However, this issue is considered and solved in our synchronization method. At the same time, the payload size is controlled well when using a confirmation signal to finalize the synchronization between LoRa nodes, which is 15 bytes in the case of this study. In view of the laboratory test presented herein, the average value of the synchronization errors of the proposed modal identification method is around 4.5 ms, which is within the

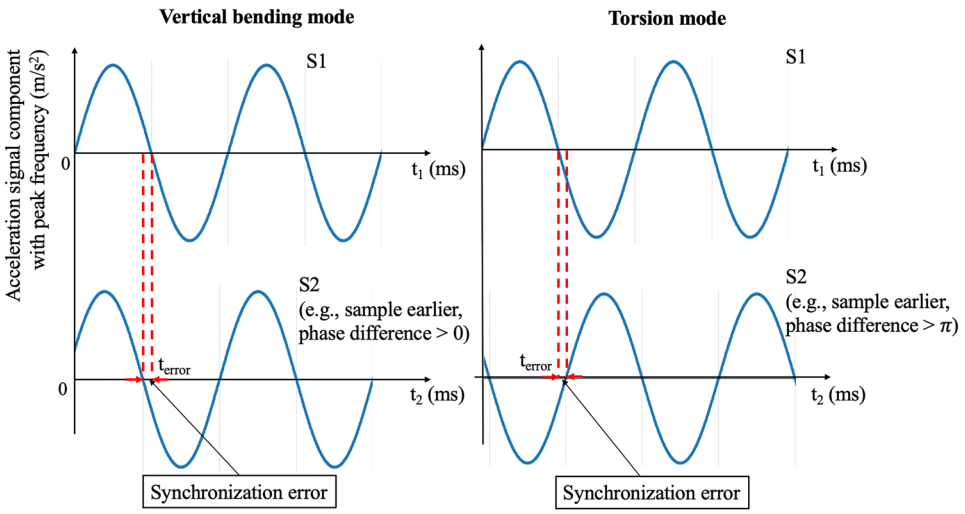

Fig. 3 Synchronization errors in modal identification

acceptable range for modal identification purposes. This will be discussed based on the laboratory test results in Sect. 3. As to the field test results, the synchronization efficiency is confirmed by the modal identification results.

The advantage of this synchronization strategy is that no timestamp resetting or correction is required from the on-board computation in the LoRa nodes, and any special format for time information is also not required in the packet transmission. Moreover, assuming full functionality of the sensor nodes, the effects of the accumulating clock drift in the sensor node itself are also decreased, as continuous synchronization is executed before each data sampling process and no clock information is involved in this synchronization strategy. As a result, LoRa packets with simple command contents and the less complicated "parse before action" protocol between the two LoRa nodes can potentially lift the success rate of wireless LoRa packet transmission. This is attributed to the fact that while using this P2P synchronization strategy, no additional confusion is introduced to the LoRa nodes when they stay in a listen state for external commands generated by LoRa signals. Moreover, this method does not require any time information from gateways or GPS signals, therefore without the need of additional hardware and avoiding power-consumptive central network-related communication. Accordingly, this synchronization strategy is very beneficial for efficient modal identification, with a unique feature on the fast initialization of LoRa end devices before synchronous measurement.

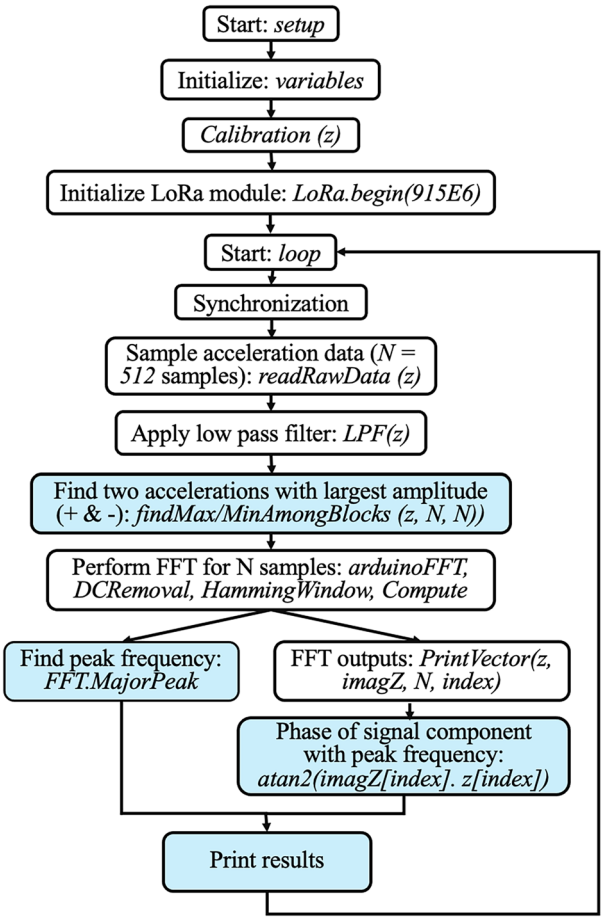

Fig. 4 Software diagram of sensor nodes

2.3 Sensor node software design for synchronous measurement

As shown in the software diagram of the sensor nodes in Fig. 4, the two LoRa sensor nodes start acceleration data sampling directly after node synchronization. Procedures to derive the output results from the two nodes are colored in blue in Fig. 4. In the data sampling part, the sensor nodes are coded with a cut-off frequency of 50 Hz and the sampling frequency of 100 Hz in accordance with Nyquist theory. As specified in multiple footbridge design codes, the fundamental frequency of common footbridges should be over the range of 3–5 Hz to avoid significant resonance with pedestrian loads [8]. Therefore, the cut-off frequency for sensor node sampling is about at least 10 times higher than the fundamental frequency of a typical footbridge, which is adequate for obtaining relatively accurate acceleration signals for FFT computation.

Within each loop, 512 acceleration data (2^9) are sampled and filtered as the input for the FFT function. Note that such a sampling number was defined to ensure reasonably fast and consecutive on-board calculation. In detail, after synchronous data sampling, a low-pass filter with a threshold frequency of 6 Hz is applied to the 512 acceleration data to decrease the influence of unexpected high-frequency electrical noise. After that, two acceleration values with the largest amplitudes in the positive and negative vertical directions are recorded to plot the maximum acceleration curves which can serve the footbridge serviceability check.

Then FFT is conducted on the 512 acceleration samples to transform time-domain data into frequency-domain outputs, and the peak frequency with the largest FFT amplitude is selected as the detected fundamental frequency. In this process, Hamming window is applied to reduce spectral leakage and to improve FFT frequency resolution. Later, to comprehend the phase information of the signal component of the fundamental frequency, the real and imaginary outputs of the FFT algorithm are retrieved with regard to the FFT length, i.e., 512. In this manner, 512 FFT amplitudes can be obtained as the square root of the sum of squares of the FFT outputs which are in the form of complex numbers. Then the FFT outputs pointing to the largest FFT amplitude are saved for phase calculation using the arctan function. As a result of this, the phase information of the fundamental frequency-based acceleration signal component can be derived from

either of the two sensor nodes, and the difference between the two phases is used for the identification of mode shape type. The whole process of synchronization, sampling, and computation takes about 6 s, and in the end, after all the results are acquired in one loop of the software diagram, both sensor nodes would get ready for the next round of synchronous measurement.

3 Experimental test results: modal identification of a beam structure

3.1 Beam test set-up

To test the functionality of the proposed modal identification method, which is based on the synchronous measurement of two LoRa nodes, a beam structure was set up to identify the fundamental frequency and potential mode shape types, targeting the vertical bending mode, the torsion mode, as well as the mixed mode that combines both of them. This beam serves as an analog for the footbridge concerned in this study. The experimental apparatus is composed of a longitudinal long beam (180 cm) made of G350 mild steel and a lateral short steel beam (85 cm), being welded orthogonally on top of the mid-span of the long beam. The dimensions of the apparatus and the test deployment method are presented in Fig. 5. The cross section of each beam is 50×6 mm, and its density is around 8063 kg/m^3. When using the LoRa nodes to identify a vertical bending mode, the long beam was fully fixed at both ends as shown in Fig. 5a, allowing the beam to vibrate up and down freely. To be able to identify a torsion mode, an additional pin support was placed underneath the welded connection of the experimental apparatus (see Fig. 5b). Specifically, a pure torsion mode can be triggered in the long beam given its large stiffness, while the short beam can act as two cantilever arms each with a sensor node and an additional weight of 2100 g at its tip (Fig. 5). Putting two sensor nodes (71 g each) on either tip was to simulate the on-site sensor placement on opposite locations across the width of the footbridge deck. When triggering a mixed mode, the beam was set up again as illustrated in Fig. 5a. Considering a typical vibration scenario on footbridges, one end of the short beam was pressed down and released freely to induce both vertical bending and torsion vibrations of the long beam. The frequencies of the vertical bending, torsion and mixed modes obtained from this test can efficiently replicate the targeted frequency values of typical footbridges.

The deployment of the experimental apparatus with sensor nodes used for identifying the vertical bending mode and the mixed mode is displayed in Fig. 6 as an example, along with the composition of the sensor node. To identify the vertical bending mode, the long beam was pressed down vertically by hand at the welded connection without the pin support. Upon a free release, the two sensor nodes could move up and down concurrently, inducing vertical vibrations of the beam. For the test on identifying the torsion mode, the temporary pin support, as indicated in Fig. 5b, was arranged under the interjection of the test beam. Specifically, lifting

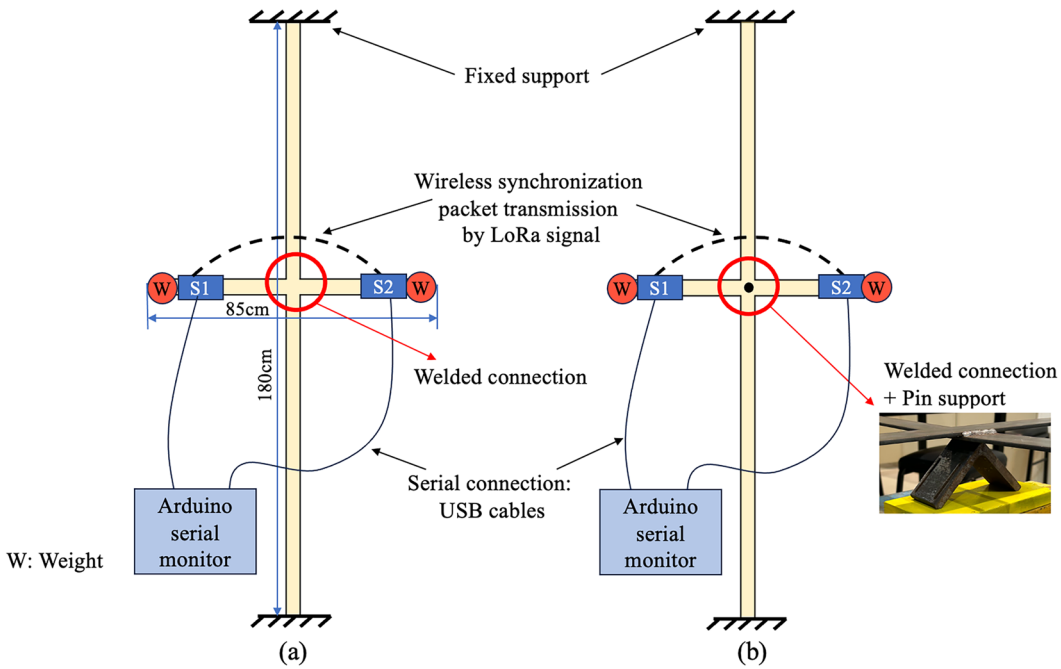

Fig. 5 Experimental set-up (top view) for modal identification of (**a**) vertical bending mode, mixed mode and (**b**) torsion mode

one end of the short beam and pressing the other one down by hand before releasing them freely can effectively twist the long beam, and the two sensor nodes can measure rotary vibrations in opposite directions. In a similar way, after removing the pin support and change the beam set-up to Fig. 5a again, the mixed mode can be tested by pressing one end of the short beam and releasing it freely.

During the test, the LoRa modules and antennas were used to perform wireless LoRa packet transmission for the synchronization of S1 and S2 before data sampling. At this stage, both nodes were connected to a laptop for result display using USB cables, and groups of results from both sensor nodes can be received from the corresponding Arduino serial monitors, as indicated in Fig. 6. After "Synched" was printed, the two sensor nodes started to measure the acceleration data simultaneously and perform FFT afterward. Subsequently, a group of results containing the result group number, the negative and positive maximum accelerations, the fundamental frequency, and the phase difference information of the sampled data were displayed line by line on the Arduino serial monitor.

A commercial Bluetooth accelerometer (WT901BLECL) was also attached next to S1 for a validation purpose of the acceleration data and frequency results obtained by the LoRa sensor nodes, with the comparison results to be presented in Sect. 3.5. The USB cables between the sensor nodes and the laptop were replaced by wireless transmission to an IoT cloud platform using the LoRaWAN protocol when applying the nodes to the footbridge field test.

3.2 Modal identification for vertical bending vibrations

Table 1 shows the modal identification results of the fundamental bending mode of the long beam when it was fixed on both ends as shown in Fig. 5a. During the test, the welded connection of the long beam was pressed down by 3 cm and released to induce vertical vibrations. This procedure was repeated after the oscillation decayed to a static status. A total of 20 groups of results were collected from S1 and S2 individually during the test time. Data recorded in the initial stage of manual excitation were excluded to eliminate the effect of hand disturbance on capturing the peak frequency and phase, as the initial vibration right after the release of hand may encompass irregular and high-frequency oscillations.

In Table 1, the synchronization timestamps, generated by the Arduino serial monitor from the laptop instead of the sensor nodes themselves, represent the actual time when synchronized data sampling began in either of the node and are used for synchronization validation. Each timestamp is accurate to millisecond, containing information of hour, minute, second and millisecond (hh:mm:ss.ms). The synchronization time error in Table 1 is the time difference between the "Sync time" of S1 and S2, and the phase difference is obtained by deducting the phase of S2 from that of S1.

From Table 1, it can be found that the synchronization time errors are either 4 or 5 ms, with an average value of 4.45 ms among 20 results. The average phase difference is 0.01 rad, which is close to the expected zero rad representing

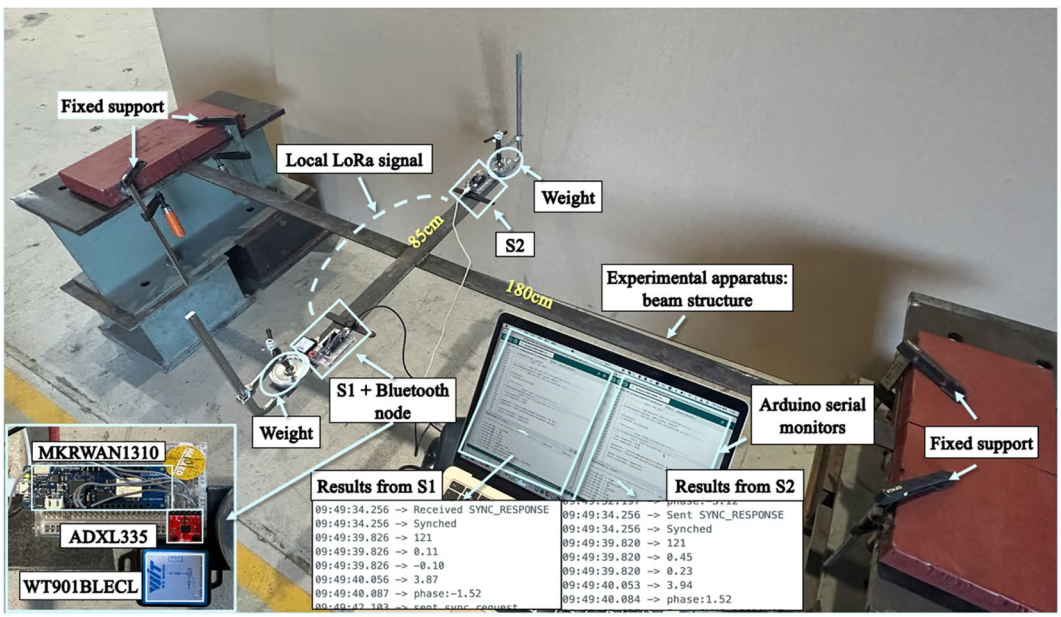

Fig. 6 Laboratory test set-up of the beam structure

Table 1 Synchronous modal identification results for vertical bending mode

Result group No	Sync time (hh:mm:ss.ms)		Time error (ms)	Fundamental frequency (Hz)		Phase (rad)		Phase diff (rad)
	S1	S2		S1	S2	S1	S2	
1	12:21:10.955	12:21:10.950	5	3.71	3.71	−1.00	−1.19	0.19
2	12:21:17.035	12:21:17.031	4	3.48	3.47	−2.35	−2.44	0.09
3	12:21:23.116	12:21:23.112	4	3.96	3.97	2.66	2.41	0.25
4	12:21:29.197	12:21:29.193	4	3.74	3.72	1.30	1.28	0.02
5	12:21:35.277	12:21:35.273	4	3.71	3.72	0.44	0.01	0.43
6	12:21:41.359	12:21:41.354	5	3.71	3.72	−0.87	−0.58	−0.29
7	12:21:47.445	12:21:47.442	5	3.72	3.49	0.45	0.69	−0.24
8	12:21:53.532	12:21:53.527	5	3.50	3.74	−0.42	−0.91	0.49
9	12:21:59.619	12:21:59.614	4	3.49	3.91	−2.12	−1.93	−0.19
10	12:22:05.699	12:22:05.695	5	3.75	3.49	2.95	2.68	0.27
11	12:22:11.779	12:22:11.774	4	3.74	3.56	1.44	1.49	−0.05
12	12:22:17.858	12:22:17.854	4	3.50	3.74	0.15	0.01	0.14
13	12:22:23.937	12:22:23.933	5	3.74	3.49	−1.22	−1.29	0.07
14	12:22:30.017	12:22:30.012	4	3.75	3.49	−2.53	−2.59	0.06
15	12:22:36.098	12:22:36.094	4	3.50	3.73	−0.27	−0.50	0.13
16	12:22:42.179	12:22:42.174	5	3.47	3.47	−2.11	−2.18	0.07
17	12:22:58.345	12:22:58.340	5	3.47	3.97	3.07	2.81	0.26
18	12:23:04.424	12:23:04.420	4	3.85	3.76	1.53	1.51	0.02
19	12:23:10.504	12:23:10.499	5	3.72	3.72	0.40	0.00	0.4
20	12:23:16.583	12:23:16.578	5	3.70	3.72	−1.10	−0.85	−0.25
Average	–		4.45	3.66	3.68	–		0.01
Standard deviation	–		–	0.14	0.16	–		–

Note: "Sync" refers to "Synchronization", "diff" refers to "difference"

a full synchronization. The phase differences are also plotted in Fig. 7a, which vary from the ideal phase difference line for the vertical bending mode. Nevertheless, these phase differences distinguish well with the ideal phase difference line for the torsion mode identification. Therefore, the combined results of time error and phase difference suggest that the synchronization strategy based on P2P LoRa communication is workable to identify a vertical bending mode (0 phase difference) from a torsion mode (π phase difference). The discrepancy to the expected zero phase difference is due to the inherent and stable time error of LoRa P2P synchronization. In addition, 512 data samples are also limited for obtaining accurate FFT frequency and phase results, leading to variation of calculated results.

Referring to Table 1 and Fig. 7b on the received fundamental frequency values, the average value from S1 is 3.66 Hz and the one from S2 is 3.68 Hz, which are very close to each other. The standard deviations of the identified frequency values from S1 and S2 are 0.14 and 0.16, respectively. The fluctuations of frequency results for S1 and S2 as well as their difference in each result group can be attributed largely to the limited data sampling number (512) used for FFT calculation, likely due to the current design of software program in relation to data processing. However, the experimental results are sufficient to prove the workability of our proposed synchronization method in identifying a vertical bending mode from a torsion mode. The relatively stable time error can be further reduced and the accuracy of the frequency results can be lifted by improving the on-board data processing capabilities in future studies.

3.3 Modal identification for torsional vibrations

Table 2 provides the results of the torsion mode identification test, during which the pin support was added under the welded connection of the experimental apparatus as presented in Fig. 5b. To trigger the torsion mode of the long beam, one end of the cantilever arm of the short beam was pressed down by 3 cm, with the other end being lifted to the same extent. Then both ends of the short beam were released simultaneously, allowing the two sensor nodes to undergo symmetric motions in opposite directions. The time error and the phase difference values in Table 2 were also calculated in the same manner as those for the vertical bending mode presented in Table 1. The negative values of phase difference are added by 2 π to keep all the phase

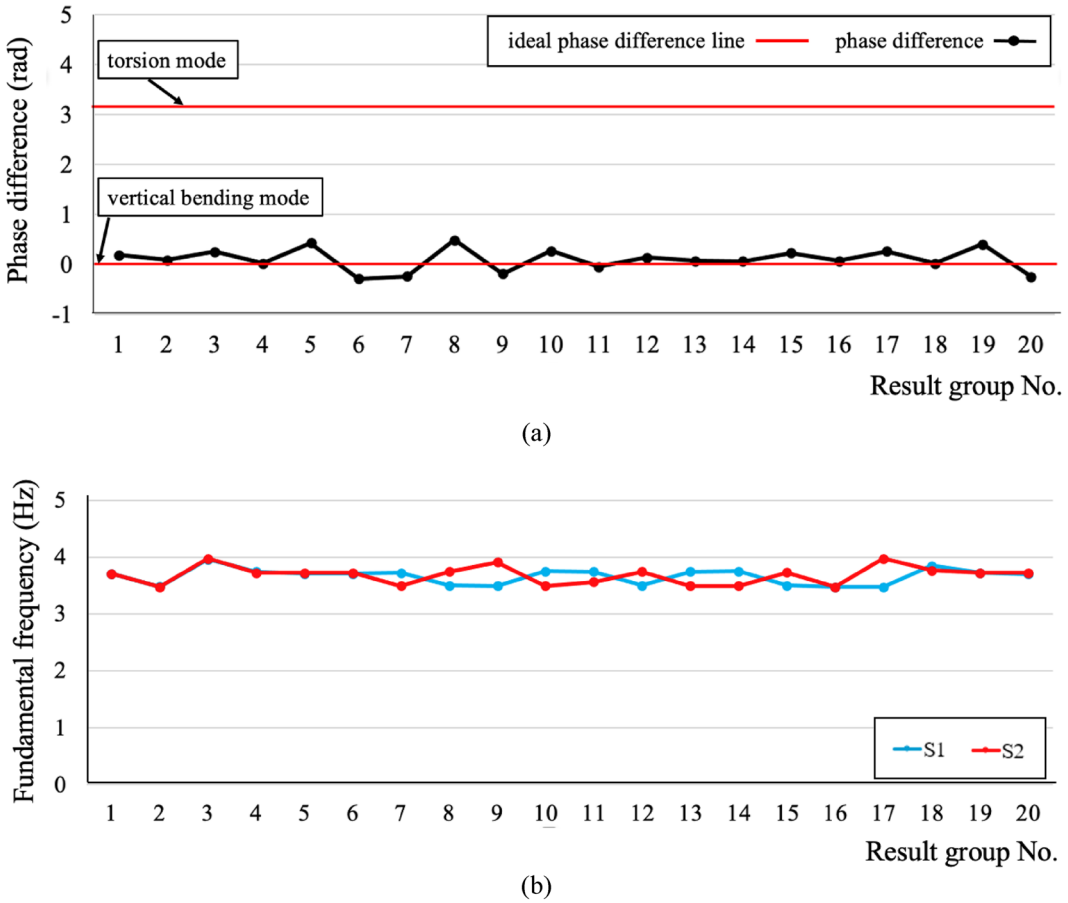

Fig. 7 Phase differences (**a**) and fundamental frequencies (**b**) of the vertical bending mode for 20 result groups

difference values in the same phase period to facilitate result analysis.

It can be noticed in Table 2 that the time errors appeared during the synchronization process were also around 4 or 5 ms as has been indicated in the vertical bending mode test, with an average value of 4.65 ms. Figure 8 gives the trend of phase differences and fundamental frequencies from 20 result groups when the long beam was oscillating under the torsion mode. The phase differences depicted in Fig. 8a are stable and very close to the ideal phase difference line for the identification of the torsion mode. Meanwhile, the phase differences are also clearly distinguishable from the ideal phase difference line of the vertical bending mode. This implies that the torsion mode is the governing vibration mode during this test. The average phase difference among 20 results is 3.02 rad, which is about 3.8% smaller than the expected phase difference of π. In relation to all the fundamental frequency results shown in Table 2 and Fig. 8b, the average frequencies are 3.63 Hz and 3.62 Hz from S1 and S2 respectively, with similar standard deviations of 0.14 from S1 and 0.15 from S2. As described above, the time error of the synchronization method is also deemed acceptable in the identification of the torsion mode from the vertical mode. The fluctuations in the frequency results from S1 and S2 as well as the difference between them in each result group indicated in Fig. 8b are also likely affected by limited data samples. These discrepancies can be rectified when more data samples are applied to perform FFT.

3.4 Modal identification for mixed vibration modes

To induce a mixed mode, potentially comprising both vertical bending and torsion modes, the experimental apparatus set-up followed the same method shown in Fig. 5a without a temporary pin support. Note that random crowds on a real footbridge can cause various modes, predominantly governed by either vertical bending mode or torsional mode. In this particular test, a typical vibration scenario was considered, in which one end of the short beam was pressed down by 3 cm and released quickly to enable both vertical and torsional vibrations.

During the beam test for the mixed modes, the LoRa nodes S1 and S2 provide 25 results from their on-board FFT calculation, required for the validation purpose presented

Table 2 Synchronous modal identification results for torsion mode

Result group No	Sync time (hh:mm:ss.ms)		Time error (ms)	Fundamental frequency (Hz)		Phase (rad)		Phase diff (rad)
	S1	S2		S1	S2	S1	S2	
1	15:35:53.740	15:35:53.736	4	3.75	3.49	− 1.83	1.44	3.01
2	15:35:59.814	15:35:59.810	4	3.49	3.74	1.10	− 1.92	3.02
3	15:36:05.889	15:36:05.884	5	3.74	3.49	− 2.16	1.10	3.02
4	15:36:11.963	15:36:11.958	5	3.49	3.74	0.95	− 2.07	3.02
5	15:36:18.036	15:36:18.031	5	3.73	3.49	− 2.19	1.07	3.02
6	15:36:24.110	15:36:24.105	5	3.49	3.73	0.99	− 2.03	3.02
7	15:36:30.184	15:36:30.179	5	3.73	3.49	− 2.09	1.18	3.01
8	15:36:36.258	15:36:36.253	5	3.49	3.73	1.14	− 1.88	3.02
9	15:36:42.329	15:36:42.325	5	3.74	3.49	− 1.91	1.36	3.01
10	15:36:48.402	15:36:48.397	5	3.49	3.74	1.34	− 1.69	3.03
11	15:36:54.475	15:36:54.470	5	3.94	3.49	− 1.68	1.58	3.02
12	15:37:00.548	15:37:00.544	4	3.72	3.94	1.59	− 1.43	3.02
13	15:37:06.622	15:37:06.617	5	3.48	3.73	− 1.41	1.86	3.01
14	15:37:12.695	15:37:12.691	4	3.73	3.48	1.87	− 1.15	3.02
15	15:37:18.767	15:37:18.763	4	3.48	3.73	− 1.15	2.12	3.01
16	15:37:24.840	15:37:24.835	5	3.73	3.48	2.11	− 0.9	3.01
17	15:37:30.912	15:37:30.908	4	3.48	3.73	− 0.89	2.38	3.01
18	15:37:36.986	15:37:36.981	5	3.73	3.48	2.42	− 0.59	3.01
19	15:37:43.060	15:37:43.055	5	3.48	3.73	− 0.56	2.71	3.01
20	15:37:49.133	15:37:49.129	4	3.73	3.48	2.76	− 0.27	3.03
Average	–		4.65	3.63	3.62	–		3.02
Standard deviation	–		–	0.14	0.15	–		–

Note: "Sync" refers to "Synchronization", "diff" refers to "difference"

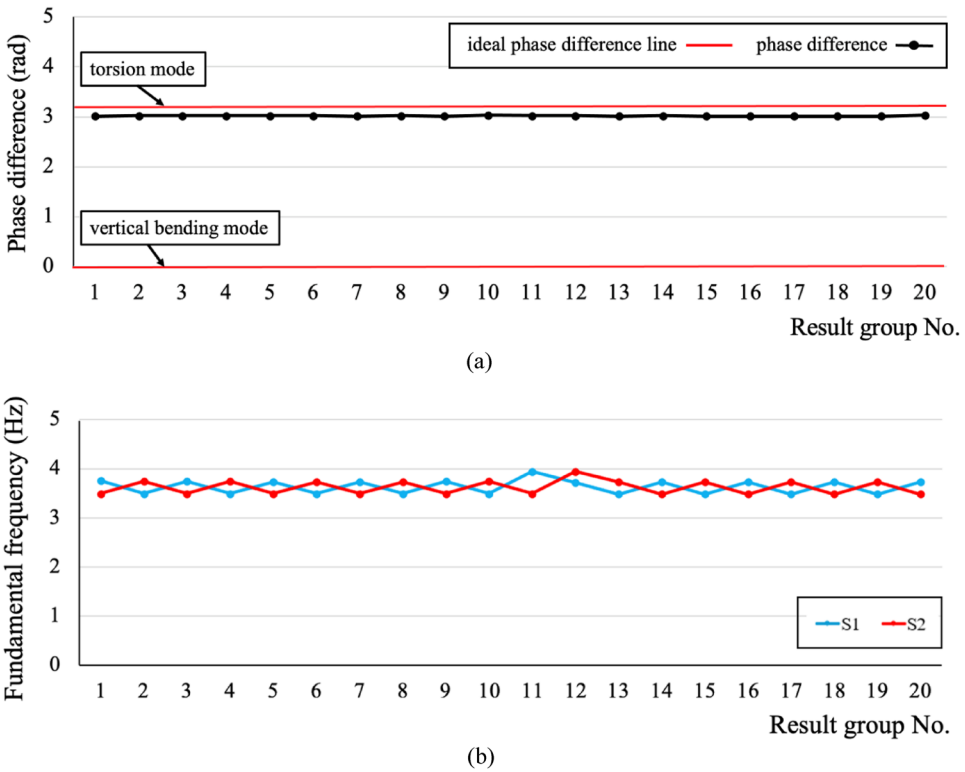

Fig. 8 Phase differences (**a**) and fundamental frequencies (**b**) of the torsion mode for 20 result groups

in Sect. 4. The modal identification results presented in Table 3 indicate that only a torsion mode with the fundamental frequency was detected all the time, as the phase differences shown in Table 3 and Fig. 9a are close to π and are far away from the ideal phase difference line of the vertical bending mode, which is 0. The average frequency values of this torsion mode are 3.6 Hz from S1 and 3.61 Hz from S2, and the standard deviations of their frequency values are 0.13 and 0.12, respectively. Limited numbers of data samples input into the on-board FFT function also lead to fluctuations of the frequency results as indicated in Fig. 9b, similar to Fig. 8b for the pure torsion mode. In the following Sect. 3.5.2, a modal analysis was conducted based on the raw acceleration data collected by one of the LoRa nodes S1, where two natural frequencies could be identified when the beam was vibrating under the mixed modes.

3.5 Validation for *LoRa* sensor node measurement

3.5.1 Maximum acceleration amplitudes from the LoRa sensor node

To verify the accuracy of the maximum acceleration amplitude results captured from the measurement of LoRa sensor nodes, a commercial Bluetooth accelerometer sensor node was attached next to S1 for a comparison (Fig. 6). The same interval of the oscillation processes for the mixed vibration modes of the experimental apparatus (Sect. 3.4) is also applied herein. The commercial WT901BLECL BLE accelerometer inclinometer can provide wireless real-time acceleration monitoring. For post-data processing, the recorded acceleration signals along the three artesian axes can be downloaded from the mobile application and sent to smartphones via Bluetooth. To maintain consistency in data sampling between both types of sensor nodes, the same

Table 3 Synchronous modal identification results for mixed modes

Result group No	Sync time (hh:mm:ss.ms)		Time error (ms)	Fundamental frequency (Hz)		Phase (rad)		Phase diff (rad)
	S1	S2		S1	S2	S1	S2	
1	15:28:23.837	15:28:23.833	4	3.48	3.73	2.84	0.51	3.95
2	15:28:29.911	15:28:29.906	5	3.74	3.48	0.99	−3.03	2.26
3	15:28:35.985	15:28:35.981	4	3.48	3.73	−2.20	0.97	3.17
4	15:28:42.059	15:28:42.054	5	3.72	3.5	1.37	−1.65	3.26
5	15:28:48.133	15:28:48.130	3	3.72	3.48	−0.98	1.75	2.73
6	15:28:54.207	15:28:54.203	4	3.48	3.73	2.66	−0.83	2.79
7	15:29:00.281	15:29:00.277	4	3.73	3.48	−0.15	2.92	3.07
8	15:29:06.355	15:29:06.351	4	3.48	3.73	−2.71	0.28	2.99
9	15:29:12.429	15:29:12.425	4	3.73	3.48	1.05	−2.36	2.87
10	15:29:19.051	15:29:19.050	1	3.49	3.73	−1.60	1.36	2.96
11	15:29:25.123	15:29:25.119	4	3.48	3.73	2.06	−1.23	2.99
12	15:29:31.200	15:29:31.196	4	3.73	3.48	−0.41	2.52	2.93
13	15:29:37.274	15:29:37.269	5	3.48	3.73	−2.99	−0.04	2.95
14	15:29:43.348	15:29:43.344	4	3.73	3.48	0.71	−2.60	2.97
15	15:29:49.421	15:29:49.417	5	3.48	3.73	−1.85	1.15	3.00
16	15:29:55.494	15:29:55.490	4	3.48	3.73	2.04	−1.30	2.94
17	15:30:01.568	15:30:01.564	4	3.73	3.48	−0.45	2.42	2.87
18	15:30:07.642	15:30:07.638	4	3.48	3.73	−3.11	−0.08	3.03
19	15:30:13.716	15:30:13.712	4	3.73	3.48	0.67	−2.64	2.97
20	15:30:19.790	15:30:19.786	4	3.48	3.73	−1.83	1.10	2.93
21	15:30:25.863	15:30:25.859	4	3.48	3.72	1.86	−1.42	3.00
22	15:30:31.937	15:30:31.932	5	3.73	3.48	−0.66	2.49	3.15
23	15:30:38.010	15:30:38.006	4	3.48	3.73	−2.83	−0.11	2.72
24	15:30:44.083	15:30:44.079	4	3.75	3.47	1.42	−2.18	2.68
25	15:30:50.155	15:30:50.150	5	3.73	3.48	−0.90	1.66	2.56
Average	–		4.08	3.60	3.61	–		2.95
Standard deviation	–		–	0.13	0.12	–		–

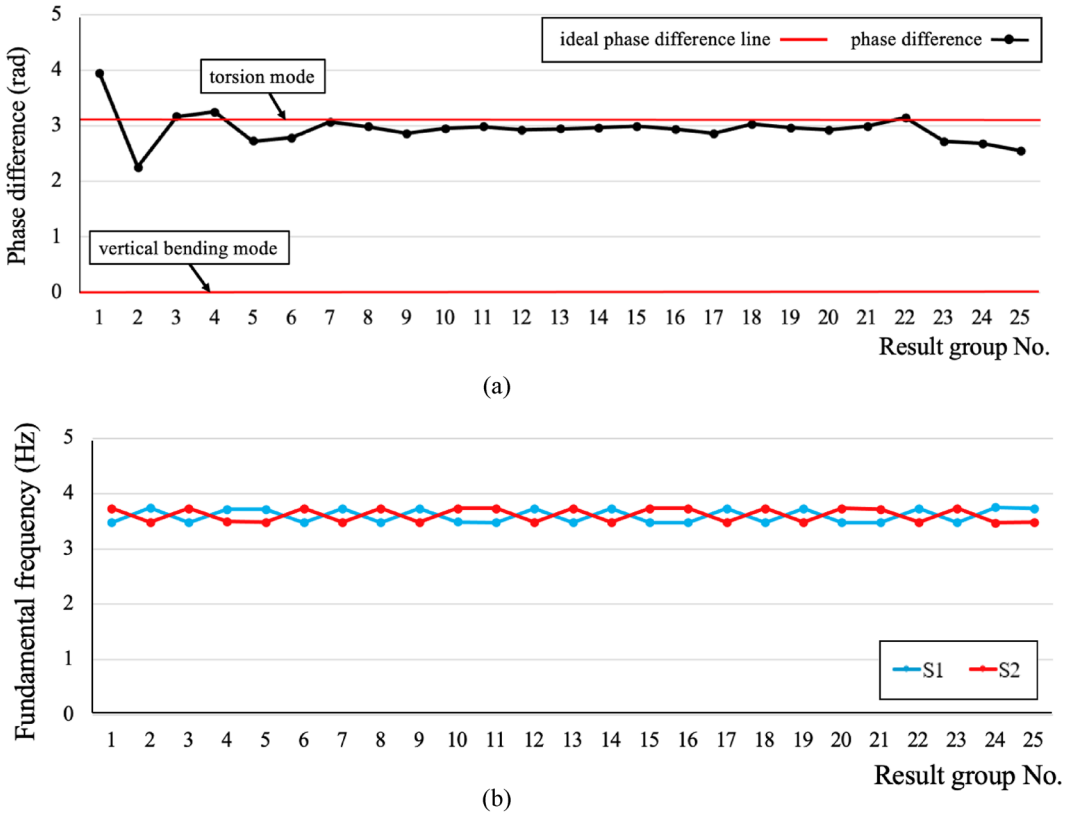

Fig. 9 Phase differences (**a**) and fundamental frequencies (**b**) of mixed modes for 25 result groups

sampling frequency of 100 Hz used for the LoRa sensor node was adopted by the Bluetooth accelerometer.

Bluetooth accelerometer performed continuous acceleration sampling, while the LoRa node only conducted sampling after the synchronization process, as indicated in its software action flow mentioned in Sect. 2.1. Therefore, during a whole term of vibration process under mixed modes induced by one-time hand excitation, Bluetooth accelerometer can collect more acceleration data compared with LoRa node.

Figure 10 presents the acceleration curves composed of the periodical maximum acceleration data with positive and negative values (red and blue dots) captured by S1 during a full round of mixed-mode oscillation, which are compared to the raw acceleration signal collected by the Bluetooth accelerometer. The Bluetooth raw data in Fig. 10 serves as a reference for the maximum accelerations captured by the LoRa node during every 5.12 s sampling window. It can be noticed that there is a discrepancy between the second pair of dots from S1 and the Bluetooth raw data. This is because LoRa sensor nodes generally record only the acceleration data with the maximum amplitudes within a fixed sampling interval. A slight difference can also be found in the first pair of maximum acceleration dots, which is attributed to the different filtering techniques used in LoRa and Bluetooth sensor nodes. Initial hand excitation on the experimental apparatus may also contribute to this difference. Overall, it can be seen in Fig. 10 that the LoRa node is able to provide relatively precise maximum acceleration results periodically, with the maximum acceleration data aligning well with the raw acceleration data from the Bluetooth sensor. Two clear curves connecting the maximum acceleration data points can thus been drawn. This agreement also indicates a rational calibration process of sensor nodes and an effective setting of sampling parameters in the preparation of synchronous LoRa sensor node measurement.

3.5.2 Fundamental frequency in the vibrating beam

For a comparison purpose on the calculated fundamental frequency results from LoRa nodes, a modal analysis was completed using a Python FFT program for the experimental apparatus. The raw acceleration signals collected by LoRa node S1 shown as an insert figure in Fig. 11a and those by the Bluetooth accelerometer in Fig. 11b are employed, which include the vibrations of the beam structure in mixed modes as outlined in Sects. 3.4. FFT analysis was used to transform time-domain signals into frequency-domain data to obtain the natural frequencies of the beam structure. The FFT spectrums derived from the raw acceleration data are

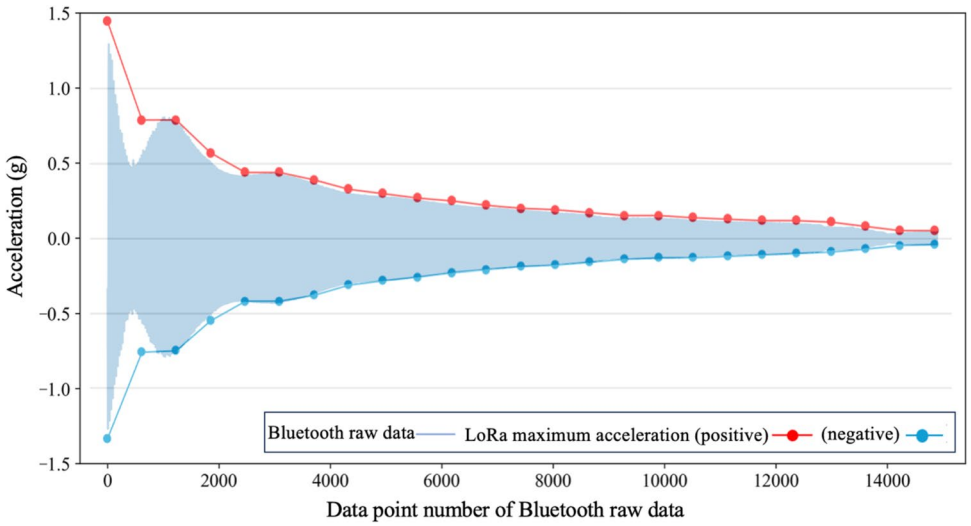

Fig. 10 Acquired acceleration data by LoRa node compared with raw acceleration signals from a commercial Bluetooth accelerometer

also presented in Fig. 11. The FFT results derived from the data recorded by the Bluetooth node in Fig. 11b display two explicit peaks (in red circles), representing two natural frequencies. On the other hand, results calculated from the raw data collected by the LoRa node in Fig. 11a demonstrate extra frequency peaks at regular intervals, in addition to the two corresponding peaks (in red circles). The reason of this phenomenon is that the raw acceleration data collected by LoRa node S1, although in a very similar pattern as those from the Bluetooth node, are not continuous as indicated in the insert figure in Fig. 11a, having regular breaks every time S1 performed the synchronization process. Therefore, the raw data being input into the FFT algorithm is not fully periodical, which can lead to periodic disturbance for the FFT calculation.

For LoRa node measurement, the two peak frequencies from the FFT spectrum shown in Fig. 11a are 3.63 Hz (torsion mode) and 3.71 Hz (bending mode), with the former being the dominant mode. For Bluetooth node measurement, Fig. 11b indicates more explicitly that the experimental apparatus was vibrating under two primary modes, with natural frequencies of 3.41 Hz (torsion mode) and 3.5 Hz (bending mode). A difference is noted between the FFT frequency results, derived from the raw acceleration data collected by both the Bluetooth and the LoRa node. Such a discrepancy could be explained by the fact that, the actual time difference between the two sampling points of the LoRa nodes may be longer than expected due to the presence of inevitable on-board data processing time. This may cause the actual sampling rate of the LoRa nodes to be less than the assumed target value (100 Hz) for FFT calculation. This could also in turn result in higher FFT frequency results than those derived from the Bluetooth data, assuming an accurate sampling rate of 100 Hz for the Bluetooth node. In future studies, to obtain a more accurate sampling rate of the LoRa nodes and thus improve the accuracy of the frequency results, improved hardware implementation with a development board having a faster and more accurate on-board processor will be adopted. This can help reduce the discrepancy between the target and actual values of the sampling rate, which can then increase the accuracy of frequency results. Moreover, with the help of improved software design in future, the actual sampling rate of the LoRa nodes can also be calculated based on its real-time data measurement conditions.

4 Field test for the synchronous *LoRa* nodes on a footbridge

The proposed modal identification method using synchronous LoRa nodes was applied to a cable-stayed footbridge to monitor its dynamic responses under random pedestrian loads. Griffith University Gold Coast campus pedestrian footbridge is 96 m long with a 4 m wide deck, comprising a 63 m main span and a 33 m back span. It has a single sloped tower of 40 m height and 5 sets of anchors to support the bridge deck. The elevation [36] and cross-sectional views of this footbridge together with the IoT system platform set-up are illustrated in Fig. 12. In order to ensure convenient wireless data transmission in the outdoor environment, each LoRa sensor node (S1 and S2) is equipped with a transmission node (T1 and T2) and a battery, composing a full LoRa node (L1 and L2). Within each LoRa node, the sensor node is responsible for sampling synchronous data with the help of P2P LoRa signals and performing on-board calculations, while the transmission node is designed to receive calculated results from the sensor node by electrical wires and forward these results to the gateway through LoRaWAN network. The two LoRa nodes were placed on opposite edges of the

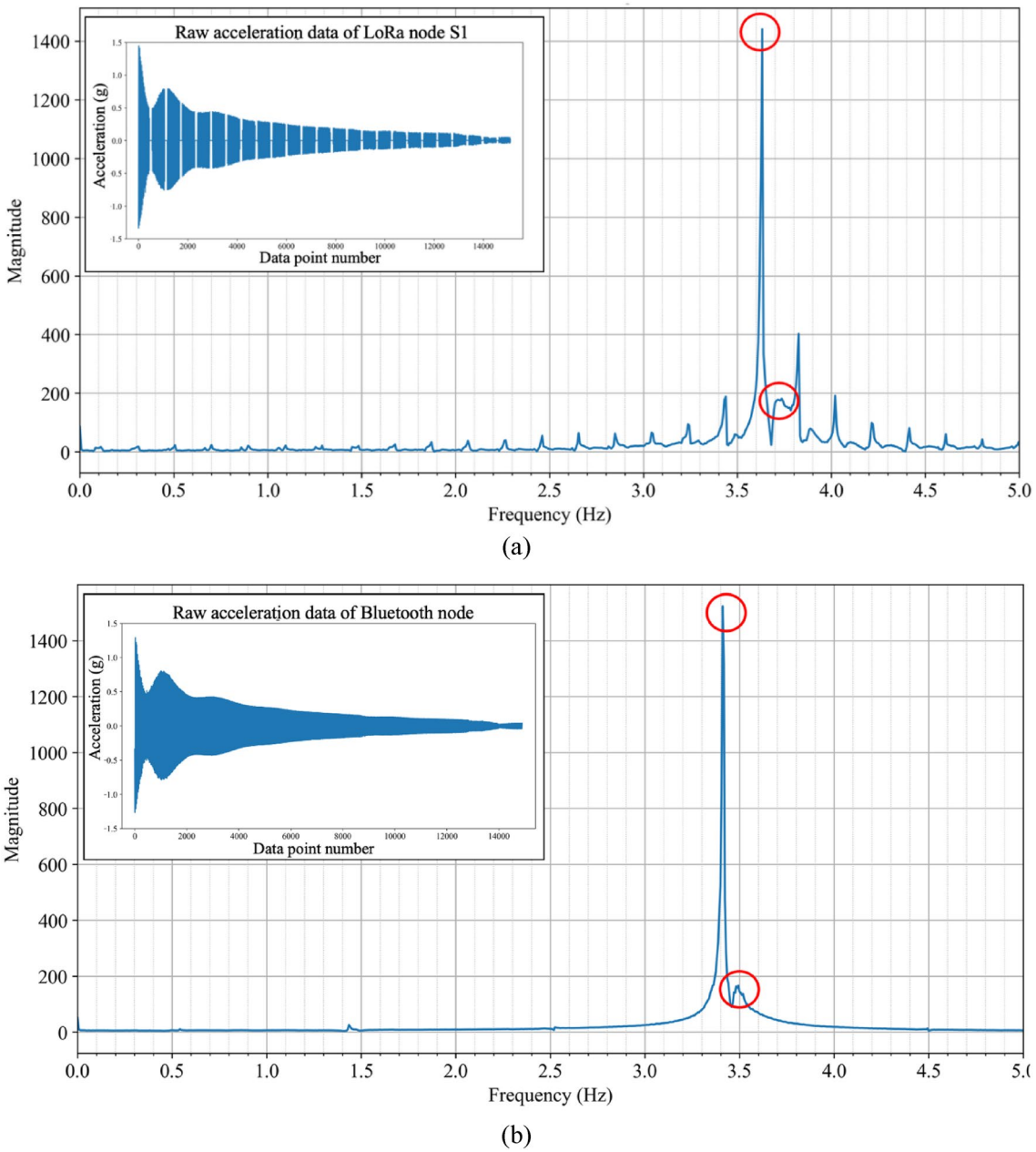

Fig. 11 FFT frequency spectrum outcomes from raw acceleration data collected by LoRa node S1 (**a**) and a commercial Bluetooth accelerometer (**b**)

deck at the locations of the first set of anchors. A portable modem was used to enable wireless data transmission from the gateway to the cloud platform via 4G cellular network given restricted Wi-Fi connection on campus. In this way, real-time data can be monitored online in the AllThingsTalk Maker [37] to track the maximum acceleration, fundamental frequency and phase of the footbridge.

Monitoring results for identifying the vibration modes of the footbridge over 15 min were retrieved online from AllThingsTalk platform and summarized in Table 4, which provide a preliminary condition monitoring of the vibrations of the footbridge. A total of 13 result groups were obtained during this time period. The phase differences are calculated from the phase collected by L1 minus that of L2. As the phase difference results shown in the table vary around zero instead of π, it can be deduced that the footbridge vibrated primarily in a vertical bending mode under the random loads from pedestrians during the test period, which was approximately 2.14 Hz on average. This frequency value is also comparable to the estimated fundamental frequency

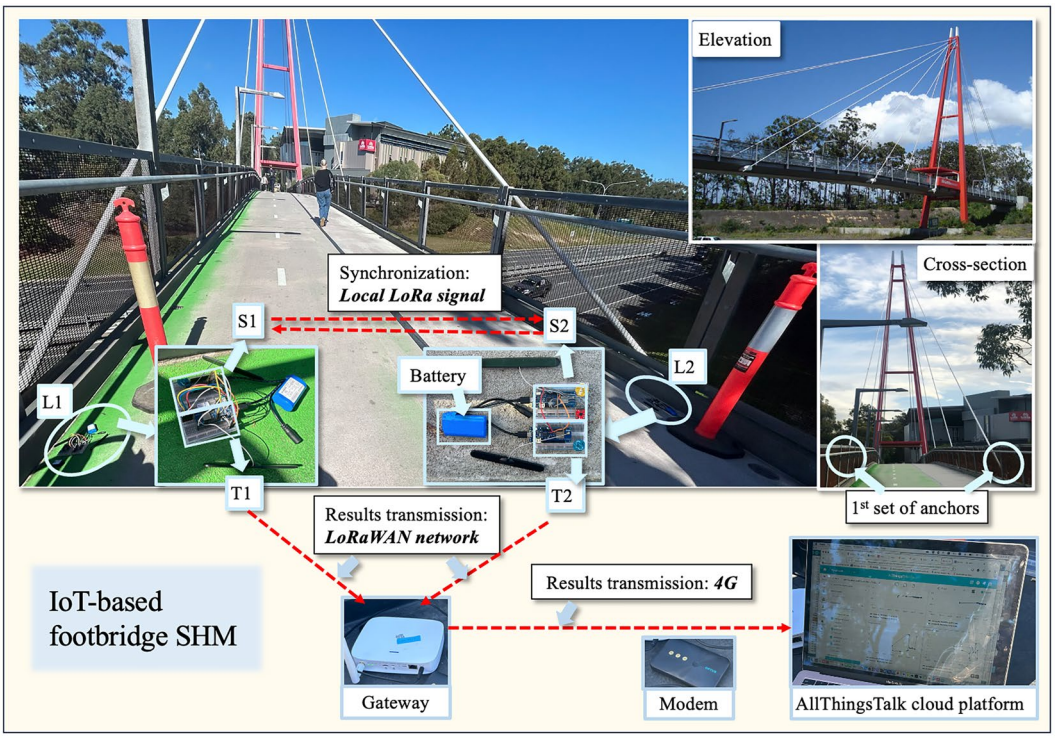

Fig. 12 Field test of synchronous LoRa nodes on a cable-stayed footbridge, with the elevation photo from [36]

in the design stage of this footbridge, which is 2.2 Hz [36]. The field test results provide evidence that the proposed modal identification method using synchronous LoRa nodes is effective in identifying the real-time dynamic responses of the footbridge, providing explicit phase difference information to confirm its first vertical bending mode. To reflect the actual vibration conditions of the footbridge, the on-board noise elimination function and FFT algorithm need to be further improved, and more sampling data need to be input into the FFT function. In future study, more frequency and phase data should be collected over a longer period of time to identify more natural frequencies and mode shapes.

The recorded acceleration data with maximum amplitudes from S1 and S2 are illustrated in Fig. 13, together with the maximum acceleration limits given in various footbridge serviceability evaluation codes, listed in Table 5. The values of maximum acceleration collected from the footbridge field test are all below 0.3 m/s^2. Considering its fundamental frequency of 2.14 Hz, it suggests that the serviceability condition of this footbridge can satisfy the maximum comfort level set by Sétra code [38], as well as the peak acceleration requirements from Euro code 5 [39] and BS 5400 [40]. Therefore, the footbridge under investigation exhibits a good condition on its vibration performance.

Table 4 Modal identification of footbridge using synchronous LoRa nodes

Result No	Fundamental frequency (Hz)		Phase (rad)		Phase difference (L1–L2, rad)
	L1	L2	L1	L2	
1	2.13	2.14	1.11	1.21	−0.10
2	2.14	2.14	−0.40	−0.31	−0.09
3	2.14	2.14	−0.05	−0.05	0.00
4	2.14	2.15	−0.27	−0.06	−0.21
5	2.12	2.13	0.63	0.67	0.04
6	2.14	2.14	−0.78	−0.78	0.00
7	2.15	2.13	−2.04	−1.65	−0.39
8	2.11	2.14	−0.95	−0.90	−0.05
9	2.12	2.13	1.14	1.17	−0.03
10	2.16	2.16	0.54	0.53	0.01
11	2.14	2.15	0.79	0.67	0.12
12	2.15	2.14	0.12	0.07	0.05
13	2.13	2.13	−0.02	−0.17	0.15

5 Conclusion

This research provides an innovation for modal identification and acceleration monitoring for wireless footbridge SHM, considering economical sensor node selection and

low-cost wireless data transmission. An effective modal identification method was proposed for vibration monitoring using LoRa sensor nodes, based on the lightweight time synchronization strategy. Peer-to-peer communication between LoRa nodes was applied to initialize synchronous measurement. Although this synchronization strategy exhibits inherent time synchronization error, it is capable of performing efficient and continuous modal identification, with the errors being within acceptable tolerances. With the help of the proposed modal identification method, the fundamental frequencies associated with a vertical bending mode, a torsion mode and combined modes can be readily determined in vibrating beam structures in an effective way. In comparison to a commercial Bluetooth accelerometer, the use of LoRa nodes is proven to develop relatively precise acceleration curves for the continuous monitoring of maximum accelerations in the laboratory test. The proposed method was also applied to a footbridge, and the fundamental frequency of the footbridge was successfully identified. The results derived from the LoRa sensor nodes were transmitted wirelessly to a gateway through LoRaWAN network and uploaded to a cloud platform, realizing long-distance, low-power footbridge monitoring. This research provides a preliminary investigation of using LoRa nodes for modal identification. For further improvement, the synchronization error can be recorded and compensated by optimizing the software design, and more sampling data need to be applied into the FFT algorithm for better frequency acquisition. In future, more sensors can be placed at the critical mode points of a footbridge to expand the monitoring system, which can subsequently provide additional modal information. To synchronize multiple sensor nodes, synchronization orders can be sent from one node to multiple nodes. Similarly, the relationship between phase and frequency results among multiple sensors can be used for modal identification of real footbridges.

Table 5 Footbridge serviceability check using various codes

Code	Frequency (f, Hz, vertical)	Maximum acceleration (m/s^2, vertical)
Sétra [38]	–	0.5 (maximum comfort level)
Euro code 5 [39]	< 5	0.7
BS 5400 [40]	< 5	$0.5f^{0.5}$

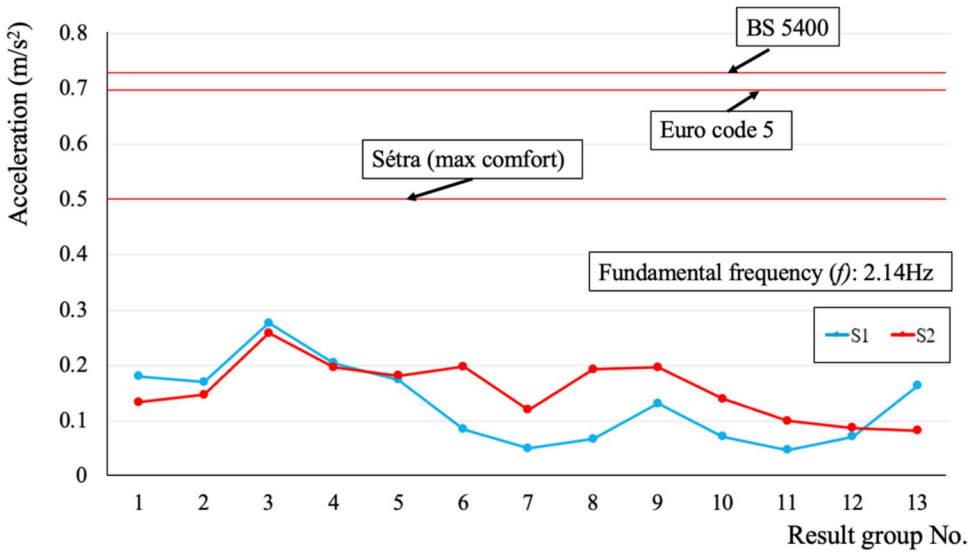

Fig. 13 Maximum acceleration data of footbridge collected by LoRa nodes

Acknowledgements The authors would like to express their sincere gratitude to the technical officers at Griffith University Engineering Laboratory for their invaluable help with test set-up and material preparation.

Funding Open Access funding enabled and organized by CAUL and its Member Institutions.

Data availability Data sharing is not applicable to this article as no new data were created or analyzed in this study.

Declarations

Competing interests The authors have no competing interests to declare that are relevant to the content of this article.

References

1. Brownjohn JMW, De Stefano A, Xu YL, Wenzel H, Aktan AE (2011) Vibration-based monitoring of civil infrastructure: challenges and successes. J Civil Struct Health Monit 1:79–95. https://doi.org/10.1007/s13349-011-0009-5
2. Figueiredo E, Brownjohn J (2022) Three decades of statistical pattern recognition paradigm for SHM of bridges. Struct Heal Monit 21(6):3018–3054. https://doi.org/10.1177/14759217221075241
3. Fan CL (2021) Detection of multidamage to reinforced concrete using support vector machine-based clustering from digital images. Struct Control Health Monit 28(12):e2841. https://doi.org/10.1002/stc.2841
4. Morgese M, Ansari F, Domaneschi M, Cimellaro GP (2020) Post-collapse analysis of Morandi's Polcevera viaduct in Genoa Italy. J Civil Struct Health Monit 10:69–85. https://doi.org/10.1007/s13349-019-00370-7
5. Carnahan H (2022) Pittsburgh bridge collapse emphasizes need for bridge repairs. J Prot Coat Linings 39(7):6–7
6. Caprani CC, Ahmadi E (2016) Formulation of human–structure interaction system models for vertical vibration. J Sound Vib 377:346–367. https://doi.org/10.1016/j.jsv.2016.05.015
7. Buffarini G, Clemente P, Giovinazzi S, Ormando C, Scafati F (2023) Structural assessment of the pedestrian bridge accessing Civita di Bagnoregio, Italy. J Civil Struct Health Monit 13:1499–1516. https://doi.org/10.1007/s13349-022-00628-7
8. Feng P, Wang Z, Jin F, Zhu S (2019) Vibration serviceability assessment of pedestrian bridges based on comfort level. J Perform Constr Facil. https://doi.org/10.1061/(asce)cf.1943-5509.0001316
9. Moser P, Moaveni B (2013) Design and deployment of a continuous monitoring system for the Dowling Hall Footbridges. Exp Tech 37:15–26. https://doi.org/10.1016/j.engstruct.2012.06.051
10. Hu WH, Moutinho C, Caetano E, Magalhães F, Cunha Á (2012) Continuous dynamic monitoring of a lively footbridge for serviceability assessment and damage detection. Mech Syst Signal Process 33:38–55. https://doi.org/10.1016/j.ymssp.2012.05.012
11. Hu WH, Caetano E, Cunha Á (2013) Structural health monitoring of a stress ribbon footbridge. Eng Struct 57:578–593. https://doi.org/10.1016/j.engstruct.2012.06.051
12. Xia Q, Wu W, Li F, Xia Y, Ding X, Lam WHK, Chung W, Xu Y (2021) System design and demonstration of performance monitoring of a butterfly-shaped arch footbridge. Struct Control Health Monit 28(7):e2738. https://doi.org/10.1002/stc.273
13. Komarizadehasl S, Huguenet P, Lozano F, Lozano-Galant JA, Turmo J (2022) Operational and analytical modal analysis of a bridge using low-cost wireless Arduino-based accelerometers. Sensors 22(24):9808. https://doi.org/10.3390/s22249808
14. De Sebastián J, Escudero A, Arnaz R, Díaz IM, Poncela A, Lorenzana A (2013) A low-cost vibration monitoring system for a stress-ribbon footbridge. In: 6th ECCOMAS Conference on Smart Structures and Materials, pp 1718–1731.
15. Feltrin G, Jalsan KE, Flouri K (2013) Vibration monitoring of a footbridge with a wireless sensor network. J Vib Control 19(15):2285–2300. https://doi.org/10.1177/1077546313501929
16. Komarizadehasl S, Lozano F, Lozano-Galant JA, Ramos G, Turmo J (2022) Low-cost wireless structural health monitoring of bridges. Sensors 22(15):5725. https://doi.org/10.3390/s22155725
17. Cruz Garcia RG, Jason K, Jastillano JD, Jones D, Manebo MB, Mark J, Aldrine F (2018) Structural health monitoring of footbridge using wireless mems accelerometers with fast Fourier transform. In: 2018 IEEE 10th International conference on humanoid, nanotechnology, information technology, communication and control, environment and management (HNICEM), Baguio City, Philippines, pp 1–4. https://doi.org/10.1109/HNICEM.2018.8666353
18. Battista de N, Brownjohn JMW, Rice JA, Sim SH, Tan HP (2013) Wireless structural monitoring of a multi-span footbridge with decentralised embedded data processing. In: the 6th International Conference on Structural Health Monitoring of Intelligent Infrastructure, Hong Kong, pp 9–11.
19. Flouri K, Bischoff R, Meyer J, Feltrin G (2013) Wireless monitoring of the dynamic performance of a footbridge. In: 2nd conference on smart monitoring, assessment and rehabilitation of civil structure.
20. Hou Z, Bao L (2023) Research and design of bridge distributed monitoring system based on lora technology. IET Wirel Sens Syst 13(3):91–103. https://doi.org/10.1049/wss2.12059
21. Farooq MO, Pesch D (2018) Analysing lora: a use case perspective. (2018). In: 2018 IEEE 4th World Forum on Internet of Things, Singapore. https://doi.org/10.1109/wf-iot.2018.8355224
22. Shanmuga Sundaram JP, Du W, Zhao Z (2020) A survey on lora networking: research problems, current solutions, and open issues. IEEE Commun Surv Tut 22(1):371–388. https://doi.org/10.1109/COMST.2019.2949598
23. Sidorov M, Khor JH, Nhut PV, Matsumoto Y, Ohmura R (2020) A public blockchain-enabled wireless Lora sensor node for easy continuous unattended health monitoring of bolted joints: implementation and evaluation. IEEE Sens J 20(21):13057–13065. https://doi.org/10.1109/jsen.2020.3001870
24. Truong TP, Duong DA, Nguyen TH, Danh LV (2020) Design and deployment of a Lora-based wireless sensor network for structural health monitoring system. Int J Smart Grid Clean Energy. https://doi.org/10.12720/sgce.10.1.83-91
25. Wang J, Zhang Y, He B, Xu J, Wei Y, Wang Y (2021) MEMS acceleration sensor vibration detection system with lora communication. In: 5th International Conference on Electronic

Information Technology and Computer Engineering. https://doi.org/10.1145/3501409.3501461
26. Qiao H, Guan H, Barber J, Nguyen TD, Jamali S, Zhu Y (2023) Preliminary investigation of vibration monitoring using long-range (LoRa) wireless network. In: 12th International Conference on Structural Health Monitoring of Intelligent Infrastructure, China
27. Maccanti M, De Lellis P, Sala A, Galli M, Giorgi M (2023) Structural monitoring: modal tracking with LoRaWAN wireless systems and automatic cloud algorithms. Lect Notes Civ Eng. https://doi.org/10.1007/978-3-031-39109-547
28. Sazonov E, Krishnamurthy V, Schilling R (2010) Wireless intelligent sensor and actuator network-a scalable platform for time-synchronous applications of structural health monitoring. Struct Heal Monit 9(5):465–476. https://doi.org/10.1177/1475921710370003
29. Singh RK, Berkvens R, Weyn M (2020) Synchronization and efficient channel hopping for power efficiency in Lora networks: a comprehensive study. Internet Things 11:100233. https://doi.org/10.1016/j.iot.2020.100233
30. De Angelis A, Santoni F, Carbone P, Cecconi M, Vecchietti A, Di Lorenzo F (2020) Development of an IoT structural monitoring system applied to a hypogeal site. Sensors 20(23):6769. https://doi.org/10.3390/s20236769
31. Ebi C, Schaltegger F, Rust A, Blumensaat F (2019) Synchronous Lora mesh network to monitor processes in underground infrastructure. IEEE Access 7:57663–57677. https://doi.org/10.1109/access.2019.2913985
32. Polonelli T, Brunelli D, Benini L (2018) Slotted aloha overlay on LoRaWAN–a distributed synchronization approach. In: 2018 IEEE 16th International Conference on Embedded and Ubiquitous Computing (EUC). https://doi.org/10.1109/euc.2018.00026
33. Haxhibeqiri J, Moerman I, Hoebeke J (2019) Low overhead scheduling of Lora transmissions for improved scalability. IEEE Internet Things J 6(2):3097–3109. https://doi.org/10.1109/jiot.2018.2878942
34. Tessaro L, Raffaldi C, Rossi M, Brunelli D (2018) Lightweight synchronization algorithm with self-calibration for Industrial Lora Sensor Networks. In: 2018 Workshop on Metrology for Industry 4.0 and IoT. https://doi.org/10.1109/metroi4.2018.8428309
35. Gao S, Zhang X, Du C, Ji Q (2019) A multichannel low-power wide-area network with high-accuracy synchronization ability for machine vibration monitoring. IEEE Internet Things J6(3):5040–5047. https://doi.org/10.1109/jiot.2019.2895158
36. Steele J, Chong L, and Newman E (2009) Griffith University Cable Stayed Pedestrian Bridge. In: Austroads Bridge Conference, 7th, 2009, Auckland, New Zealand.
37. Allthingstalk Maker (2024) https://maker.allthingstalk.com
38. Sétra F (2006) Assessment of vibrational behaviour of footbridges under pedestrian loading. Technical guide SETRA, Paris, France.
39. ECS (1997) Eurocode 5: design of timber structures—part 2: bridges (ENV 1995- 2).European Committee for Standardization.
40. BSI (1978) Steel, concrete and composite bridges—part 2: specification for Loads. British Standards Association, London

Terms and Conditions

Springer Nature journal content, brought to you courtesy of Springer Nature Customer Service Center GmbH (“Springer Nature”).
Springer Nature supports a reasonable amount of sharing of research papers by authors, subscribers and authorised users (“Users”), for small-scale personal, non-commercial use provided that all copyright, trade and service marks and other proprietary notices are maintained. By accessing, sharing, receiving or otherwise using the Springer Nature journal content you agree to these terms of use (“Terms”). For these purposes, Springer Nature considers academic use (by researchers and students) to be non-commercial.
These Terms are supplementary and will apply in addition to any applicable website terms and conditions, a relevant site licence or a personal subscription. These Terms will prevail over any conflict or ambiguity with regards to the relevant terms, a site licence or a personal subscription (to the extent of the conflict or ambiguity only). For Creative Commons-licensed articles, the terms of the Creative Commons license used will apply.
We collect and use personal data to provide access to the Springer Nature journal content. We may also use these personal data internally within ResearchGate and Springer Nature and as agreed share it, in an anonymised way, for purposes of tracking, analysis and reporting. We will not otherwise disclose your personal data outside the ResearchGate or the Springer Nature group of companies unless we have your permission as detailed in the Privacy Policy.
While Users may use the Springer Nature journal content for small scale, personal non-commercial use, it is important to note that Users may not:

1. use such content for the purpose of providing other users with access on a regular or large scale basis or as a means to circumvent access control;
2. use such content where to do so would be considered a criminal or statutory offence in any jurisdiction, or gives rise to civil liability, or is otherwise unlawful;
3. falsely or misleadingly imply or suggest endorsement, approval , sponsorship, or association unless explicitly agreed to by Springer Nature in writing;
4. use bots or other automated methods to access the content or redirect messages
5. override any security feature or exclusionary protocol; or
6. share the content in order to create substitute for Springer Nature products or services or a systematic database of Springer Nature journal content.

In line with the restriction against commercial use, Springer Nature does not permit the creation of a product or service that creates revenue, royalties, rent or income from our content or its inclusion as part of a paid for service or for other commercial gain. Springer Nature journal content cannot be used for inter-library loans and librarians may not upload Springer Nature journal content on a large scale into their, or any other, institutional repository.
These terms of use are reviewed regularly and may be amended at any time. Springer Nature is not obligated to publish any information or content on this website and may remove it or features or functionality at our sole discretion, at any time with or without notice. Springer Nature may revoke this licence to you at any time and remove access to any copies of the Springer Nature journal content which have been saved.
To the fullest extent permitted by law, Springer Nature makes no warranties, representations or guarantees to Users, either express or implied with respect to the Springer nature journal content and all parties disclaim and waive any implied warranties or warranties imposed by law, including merchantability or fitness for any particular purpose.
Please note that these rights do not automatically extend to content, data or other material published by Springer Nature that may be licensed from third parties.
If you would like to use or distribute our Springer Nature journal content to a wider audience or on a regular basis or in any other manner not expressly permitted by these Terms, please contact Springer Nature at

onlineservice@springernature.com